# Accepted Manuscript

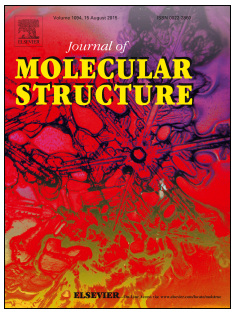


DNA binding propensity and nuclease efficacy of biosensitive Schiff base complexes containing pyrazolone moiety: Synthesis and characterization

Rajakkani Paulpandiyan, Natarajan Raman

PII: S0022-2860(16)30674-3

DOI: 10.1016/j.molstruc.2016.07.003

Reference: MOLSTR 22706

To appear in: *Journal of Molecular Structure*

Received Date: 13 May 2016

Revised Date: 30 June 2016

Accepted Date: 1 July 2016

Please cite this article as: R. Paulpandiyan, N. Raman, DNA binding propensity and nuclease efficacy of biosensitive Schiff base complexes containing pyrazolone moiety: Synthesis and characterization, *Journal of Molecular Structure* (2016), doi: 10.1016/j.molstruc.2016.07.003.

# DNA binding propensity and nuclease efficacy of biosensitive Schiff base complexes containing pyrazolone moiety: Synthesis and characterization

**Rajakkani Paulpandiyan and Natarajan Raman***

*Research Department of Chemistry, VHNSN College, Virudhunagar-626 001, India

*E-mail: ramchem1964@gmail.com; Tel.: +091-092451-65958; Fax: +091-4562-28133*

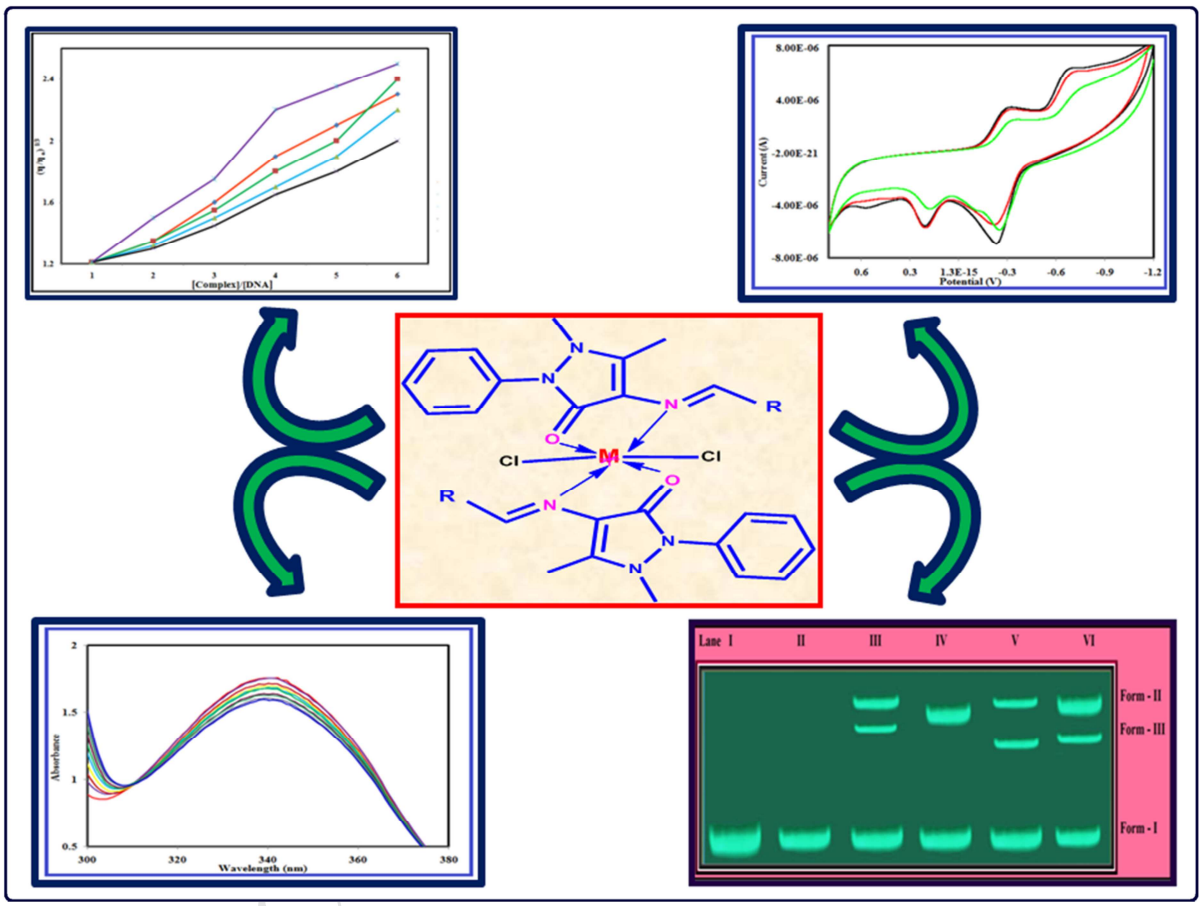

# DNA binding propensity and nuclease efficacy of biosensitive Schiff base complexes containing pyrazolone moiety: Synthesis and characterization

**Rajakkani Paulpandiyan and Natarajan Raman***

*Research Department of Chemistry, VHNSN College, Virudhunagar-626 001, India

*E-mail: ramchem1964@gmail.com; Tel.: +091-092451-65958; Fax: +091-4562-281338*

---

ABSTRACT

---

A series of novel Co(II), Cu(II), Ni(II) and Zn(II) complexes (**1-8**) were synthesized from pyrazolone precursor Schiff base(s), obtained by the condensation of 4-amino-2,3-dimethyl-1-phenyl-3-pyrazolin-5-one (4–aminoantipyrine) with cinnamaldehyde/benzaldehyde and respective metal(II) chloride. They have been characterized by elemental analysis, magnetic susceptibility, molar conductance measurements, UV-Vis., IR, NMR, ESI mass spectra and EPR studies. These complexes show lower conductance values, supporting their non-electrolytic nature. Spectroscopic and other analytical data of the complexes suggest octahedral geometry. The binding properties of these complexes with DNA have been explored by electronic absorption spectra, cyclic voltammetry and viscosity measurements which reveal that the complexes have the ability to interact with calf thymus DNA (CT DNA) by intercalative mode. The binding constant ($K_b$) values clearly signify that the complex **1** has more intercalating ability than other complexes. DNA cleavage efficacy of these complexes with pUC18 DNA has been investigated by gel electrophoresis technique. All the complexes have been found to promote cleavage of pUC18 DNA from the super coiled form I to the open circular form II in presence of hydrogen peroxide. The *in vitro* antibacterial and antifungal assay, investigated by Minimum Inhibitory Concentration (MIC) method indicates that these complexes are good antimicrobial agents against various pathogens.

---

**Keywords:** Pyrazolone precursor Schiff base; non-electrolytic nature; octahedral geometry; DNA cleavage efficacy; supercoiled form; antimicrobial agents.

---

## 1. Introduction

Schiff bases intrigue attention of coordination chemists as versatile spacers due to their viable accessibilities and structural diversity [1-2]. These are essential class of ligands based on their synthetic feasibility, selectivity and coordinative ability towards the central metal atom as well as the structural feature resemble to biological moiety. In particular, any ligand possess azomethine group (-HC=N-) reveal significance as 'privileged ligands'. The availability of lone pair of electrons in $sp^2$ hybridized orbital of nitrogen atom in azomethine group extensively participate to excel its chelation effect, while exploring *via* cooperation of one or more donor centers adjacent to azomethine group. Schiff bases afford to form stable complexes with majority of transition metal ions and sequester in various oxidation states. Contemporarily, many groups engaged with the synthesis and characterization of transition metal chelates of pyrazolone derivatives. Amidst the pyrazolone derivatives, 4-aminoantipyrine occupies a prominent role due to its importance in biological, pharmacological, clinical and analytical applications [3-6]. It has been ventured as an analgesic, anti-inflammatory and anti-pyretic agent, later replaced due to its influence of agranulocytosis side effect which is an acute condition associated with insensitive and precarious leukopenia (lowered white blood cell count), most commonly the neutrophils caused by neutropenia in the circulating blood. It leads to the deficiency of major class of infection-fighting white blood cells. Human beings undergo this condition by experiencing the risk of infections due to the suppressed immunity [7]. Alternatively, research is initiated with derivatives of 4-aminoantipyrine to reduce the toxicity of those derivatives as drug candidates. Recently, 4-aminoantipyrine derivatives are employing to exhibit remarkable properties like multi-site coordination [8], anti-oxidant [9] anti-putrefactive [10] and optical characteristics [11] in chemical and material science. On this basis, it is essential to choose 4-aminoantipyrine as a precursor in this research field.

Since the microbes are developing resistance to antibiotics available in practice, demands the search for the improved compound with potential effects against pathogenic bacteria. In this context, impressive progress in medicinal chemistry has been accomplished using aromatic aldehydes which occupied as critical entity in regulating biological activities. Parekh and co-workers reported the synthesis of Schiff bases derived from 4-aminobenzoic acid and cinnamaldehyde [12]. These were identified as potential antibacterial agents against a number of

medically important bacterial strains. The above results prompted us to choose cinnamaldehyde and benzaldehyde as reagents for preparing the Schiff bases.

Towards the objective of achieving a promising results from the above substrates, we have succeeded with the synthesis of two different Schiff base ligands from 4-aminoantipyrine with cinnamaldehyde/benzaldehyde ($L^1$/$L^2$). These Schiff base ligands are explored to coordinate with Cu(II), Co(II), Ni(II) and Zn(II) metal ions to afford a series of metal complexes (**1-8**). Both free ligands and the corresponding complexes were characterized by physicochemical and variety of spectroscopic techniques. Ultimately, their collective and functional biological properties were analyzed by *in vitro* antimicrobial bustle, DNA binding and DNA cleavage using gel electrophoresis.

## 2. Materials and Methods

The chemicals and reagents used were of Analar grade and used as such without further purification. However, the solvents were purified by the standard procedure. Cinnmaldehyde and benzaldehyde were procured and used as received from SD fine products. 4- aminoantipyrine and all other metal salts were supplied by Merck Chemicals.

Elemental analysis (C, H and N) data were carried out in Perkin-Elmyer 240 elemental analyzer. Vibrational spectral data were collected from FT IR–Shimadzu model IR-Affinity-1 spectrophotometer using KBr discs. $^1$H NMR and $^{13}$C NMR of ligands and their Zn(II) complexes were recorded with Bruker 400MHz Avance III HD Nanobay NMR spectrometer using DMSO-$d_6$ as the deuterated solvent. Mass spectrometry experiments were performed in JEOL-AccuTOF JMS-T100LC mass spectrometer equipped with a custom-made electrospray interface (ESI). The room temperature molar conductivity of complexes in DMSO solution ($10^{-3}$ M) was measured using a deep vision 601 model digital conductivity meter. The X-band EPR spectrum was recorded at LNT (77 K) and room temperature (300 K). Absorption spectra were recorded using UV-Vis spectrophotometer, Shimadzu model UV-1601 at room temperature. Cyclic voltammetric (CV) experiments were conducted in CHI 620C electrochemical analyzer in freshly distilled DMSO solution.

*2.1 Synthesis*

*2.1.1 Synthesis of Schiff base ligand ($L^1$/$L^2$)*

Schiff bases ($L^1$/$L^2$) were synthesized by adopting the synthetic procedure reported in literature from our research group [13]. 4-amino-2,3-dimethyl-1-phenyl-3-pyrazolin-5-one (4-aminoantipyrine) (2.03 g, 10 mmol) in 40 mL of ethanol was stirred with cinnamaldehyde (1.32 g, 10 mmol, $L^1$) / benzaldehyde (1.06 g, 10 mmol, $L^2$) in 1:1 molar ratio at ambient temperature by magnetic stirrer for *ca.* 1 h. The Schiff base 4-cinnamylimino-2, 3-dimethyl-1-phenyl-3-pyrazal-5-one (**$L^1$**)/ 4-benzylimino-2,3-dimethyl-1-phenyl-3-pyrazal-5-one (**$L^2$**) formed as orange solid, was isolated by filtration and washed with ethanol followed by an excess of petroleum-ether to eliminate any unreacted reagent. After washing the product for three times, compound was recrystallized from ethanol to obtain a pure solid and dried over anhydrous calcium chloride in desiccator under mild *vacuum.* Thus, the formation of Schiff base ligands $L^1$ and $L^2$ is displayed in Scheme 1.

(Kindly insert **Scheme 1** here)

**[$L^1$]** Yield: 80%; orange colour; Anal.Calc.for $C_{20}H_{19}N_3O$ (%) C (75.6), H (5.8), N (13.0); Found (%): C (74.1), H (5.1) and N (12.6); FT-IR (KBr) ($cm^{-1}$): 1595 (-CH=N), 492 (-CH=CH-) and 1674 (C=O); $^1$H NMR (DMSO-$d_6$) δ ppm: 7.0-7.6 (m,Ar-H), 2.4 (s,-C-$CH_3$), 3.2 (s,-N-$CH_3$), 6.6 (s,-CH=CH-), 9.6 (s,-CH=N); $^{13}$C NMR (DMSO-$d_6$) δ ppm: 125-130 (Ar-C), 135 (-HC=CH), 160 (-CH=N), 152 (C=O) 10.2 (-C-$CH_3$), 35.8 (-N-$CH_3$); UV-Vis in DMSO, $cm^{-1}$ (transition): 35714 (π-π*) and 29498 (n-π*)

**[$L^2$]** Yield: 68%; Pale orange colour; Anal.Calc.for $C_{18}H_{17}N_3O$ (%) C (74.2), H (5.8), N (14.4); Found (%): C (73.6), H (5.2) and N (14.0); FT-IR (KBr) ($cm^{-1}$): 1590 (-CH=N), and 1678(C=O); $^1$H NMR (DMSO-$d_6$) δ ppm: 7.0-7.6 (m,Ar-H), 2.4 (s,-C-$CH_3$), 3.2 (s,-N-$CH_3$), 9.6 (s,-CH=N); $^{13}$C NMR (DMSO-$d_6$) δ ppm: 125-130 (Ar-C), 160 (-CH=N), 152 (C=O) 10.2 (-C-$CH_3$), 35.8 (-N-$CH_3$); UV-Vis in DMSO, $cm^{-1}$ (transition): 35622 (π-π*) and 28952 (n-π*)

*2.1.2 Synthesis of metal complexes*

Cu(II), Co(II), Ni(II) and Zn(II) complexes were prepared by the addition of molar quantity of ligand with respect to stoichiometry of metal salts using the following procedure. A solution of metal(II) chloride in ethanol (2 mmol) was stirred with an ethanolic solution of 4-cinnamylimino-2,3-dimethyl-1-phenyl-3-pyrazal-5-one ($L^1$)/4-Benzylimino-2,3-dimethyl-1-phenyl-3-pyrazal-5-one ($L^2$) (4 mmol) in 1:2 molar ratio, using magnetic stirrer at ambient

temperature for 30 min and then refluxed for *ca.* 3 h. Then the volume of the reaction mixture was reduced to one-third using water bath and cooled. The solid product formed was filtered, recrystallized from ethanol and dried in *vacuo*. Schematic route for the synthesis of metal complexes (**1-8**) using the above Schiff base ligands ($L^1/L^2$) are exemplified in Scheme 2.

(Kindly insert **Scheme 2** here)

**[$CuL^1_2Cl_2$] (1):** Yield: 65 %; Brown colour; Anal. Calc. for $CuC_{40}H_{38}N_6O_2Cl_2$ (%): C (62.4), H (4.9), N (10.9) and Cu (8.2); Found (%): C (61.1), H (4.2), N (10.0) and Cu (8.0); FT-IR (KBr) ($cm^{-1}$): 1580 (-CH=N), 1654 (C=O), 1492 (-CH=CH-), 365 (M-Cl), 507 (M-O) and 464 (M-N); $\Lambda_m$ ($\Omega^{-1}mol^{-1}cm^2$) 14.0; $\mu_{eff}$ (BM) 1.84; UV-Vis in DMSO, $cm^{-1}$ (transition): 14,836 $cm^{-1}$ (d-d).

**[$CoL^1_2Cl_2$] (2):** Yield: 62%; Green colour; Anal.Calc for $CoC_{40}H_{38}N_6O_2Cl_2$ (%): C (62.8), H (4.9), N (10.9) and Co (7.7); Found (%): C (62.0), H (4.2), N (10.1) and Co (7.1); FT-IR (KBr) ($cm^{-1}$): 1575 (-CH=N), 1645 (-C=O), 1492 (-CH=CH-), 360 (M-Cl), 505 (M-O) and 455 (M-N); $\Lambda_m$ ($\Omega^{-1}mol^{-1}cm^2$) 18.0; $\mu_{eff}$ (BM) 4.65; UV-Vis in DMSO, $cm^{-1}$(transition): 13,247 $cm^{-1}$ (d-d).

**[$NiL^1_2Cl_2$] (3):** Yield: 68%; Brownish yellow colour; Anal.Calc for $NiC_{40}H_{38}N_6O_2Cl_2$ (%): C (62.8), H (4.9), N (10.9) and Ni (7.6); Found (%): C (62.1), H (4.2), N (10.1) and Ni (7.0); FT-IR (KBr) ($cm^{-1}$) 1578 (-CH=N), 1664 (C=O), 1492 (-CH=CH-), 372 (M-Cl), 512 (M-O) and 458 (M-N); $\Lambda_m$ ($\Omega^{-1}mol^{-1}cm^2$) 12.0; $\mu_{eff}$ (BM) 3.12; UV-Vis in DMSO, $cm^{-1}$ (transition): 12,826 $cm^{-1}$ (d-d).

**[$ZnL^1_2Cl_2$] (4):** Yield: 70%; Greenish yellow colour; Anal.Calc for $ZnC_{40}H_{38}N_6O_2Cl_2$ (%): C (62.3), H (4.9), N (10.9) and Zn (8.5); Found (%) : C (61.5), H (4.2), N (10.2) and Zn (8.0); FT-IR (KBr) ($cm^{-1}$): 1580 (-CH=N), 1652 (C=O), 1492 (-CH=CH-), 374 (M-Cl), 515 (M-O) and 460 (M-N); $^1H$ NMR (DMSO-$d_6$) δ ppm: 7.0-7.6 (m, Ar-H), 2.4 (s,-C-$CH_3$), 3.2 (s,-N-$CH_3$), 6.6 (s,-CH=CH-), 9.4 (s,-CH=N); $^{13}C$ NMR (DMSO-$d_6$) δ ppm: 124-130 (Ar-C), 157 (-CH=N), 144 (C=O), 135 (-HC=CH-), 10.2 (-C-$CH_3$) and 35.8 (-N-$CH_3$); $\Lambda_m$ ($\Omega^{-1}mol^{-1}cm^2$) 10.0; $\mu_{eff}$ (BM) diamagnetic; UV-Vis in DMSO, $cm^{-1}$ (transition): 27,654 (LMCT).

**[CuL$^2_2$Cl$_2$] (5):** Yield: 68%; Dark brown colour; Anal. Calc. for $CuC_{36}H_{34}N_6O_2Cl_2$ (%): C (60.4), H (4.7), N (11.7) and Cu (9.9); Found (%): C (60.1), H (4.2), N (11.0) and Cu (9.2); FT-IR (KBr) (cm$^{-1}$): 1576 (-CH=N), 1652 (C=O), 360 (M-Cl), 509 (M-O) and 468 (M-N); $\Lambda_m$ ($\Omega^{-1}$mol$^{-1}$cm$^2$) 12.0; $\mu_{eff}$ (BM) 1.86; UV-Vis in DMSO, cm$^{-1}$ (transition): 14,928 cm$^{-1}$ (d-d).

**[CoL$^2_2$Cl$_2$] (6):** Yield: 66%; Green colour; Anal. Calc. for $CoC_{36}H_{34}N_6O_2Cl_2$ (%): C (60.8), H (4.8), N (11.7) and Co (8.3); Found (%): C (60.2), H (4.2), N (11.1) and Co (8.1); FT-IR (KBr) (cm$^{-1}$): 1580 (-CH=N), 1664 (-C=O), 368 (M-Cl), 512 (M-O) and 464 (M-N); $\Lambda_m$ ($\Omega^{-1}$mol$^{-1}$cm$^2$) 20.0; $\mu_{eff}$ (BM) 4.62; UV-Vis in DMSO, cm$^{-1}$ (transition): 13,456 cm$^{-1}$ (d-d).

**[NiL$^2_2$Cl$_2$] (7):** Yield: 60%; yellow colour; Anal.Calc for $NiC_{36}H_{34}N_6O_2Cl_2$ (%): C (60.8), H (4.9), N (11.7) and Ni (8.2); Found (%): C (60.1), H (4.2), N (11.1) and Ni (8.0); FT-IR (KBr) (cm$^{-1}$) 1572 (-CH=N), 1678 (C=O), 368 (M-Cl), 510 (M-O) and 452 (M-N); $\Lambda_m$ ($\Omega^{-1}$mol$^{-1}$cm$^2$) 13.0; $\mu_{eff}$ (BM) 3.35; UV-Vis in DMSO, cm$^{-1}$ (transition): 12,654 cm$^{-1}$ (d-d).

**[ZnL$^2_2$Cl$_2$] (8):** Yield: 74%; Pale yellow colour; Anal.Calc for $ZnC_{36}H_{34}N_6O_2Cl_2$ (%): C (60.1), H (4.7), N (11.7) and Zn (9.1); Found (%) : C (59.5), H (4.2), N (11.2) and Zn (9.0); FT-IR (KBr) (cm$^{-1}$): 1570 (-CH=N), 1656 (C=O), 370 (M-Cl), 510 (M-O) and 462 (M-N); $^1$H NMR (DMSO-$d_6$) δ ppm: 7.0-7.6 (m, Ar-H), 2.4 (s,-C-CH$_3$), 3.2 (s,-N-CH$_3$), 9.4 (s,-CH=N); $^{13}$C NMR (DMSO-$d_6$) δ ppm: 124-130 (Ar-C), 157 (-CH=N), 144 (C=O), 10.2 (-C-CH$_3$) and 35.8 (-N-CH$_3$); $\Lambda_m$ ($\Omega^{-1}$mol$^{-1}$cm$^2$) 16.0; $\mu_{eff}$ (BM) diamagnetic; UV-Vis in DMSO, cm$^{-1}$ (transition): 27,892 (LMCT).

*2.3. DNA binding studies*

The DNA-binding experiments were conducted at ambient temperature. Electronic absorption spectroscopic method has been adopted to investigate the relative bindings of these complexes to CT DNA in the medium of 5 mM Tris–HCl/NaCl buffer (pH = 7.2). As such the solution of CT DNA exhibited a ratio of UV absorbance at 260 and 280 nm, $A_{260}/A_{280}$ = 1.8–1.9, indicating the existence of DNA, adequately free of protein [14]. The CT DNA stock solution was prepared in 5 mM Tris–HCl/ 50 mM NaCl buffer (pH = 7.2, stored at 4 ºC and used within 4

days of preparation). The concentration of CT DNA was determined from its absorption intensity at 260 nm with a molar extinction coefficient of 6600 $M^{-1}$ $cm^{-1}$ [15, 16].

*2.3.1. Electronic absorption spectroscopic studies*

The electronic absorption spectra of these complexes were recorded before and after the addition of DNA in the medium of 5 mM Tris-HCl/50 mM NaCl buffer (pH 7.2). The intrinsic binding constant for the interaction of each complex with DNA was obtained from the absorption data. The absorption titrations were carried out by the addition of variable amount of DNA into the solution of the complex (keeping its concentration as constant) taken in a quartz cell. The titration process was repeated until the disappearance of change in the spectra, suggesting the binding saturation. The intrinsic binding constant $K_b$ was determined from the plot of [DNA]/($\varepsilon_a$- $\varepsilon_f$) *vs*. [DNA] according to equation (3).

$$[DNA]/ (\varepsilon_a - \varepsilon_f) = [DNA]/ (\varepsilon_b - \varepsilon_f) + 1/[K_b(\varepsilon_b - \varepsilon_f)] \text{ ---------- (3)}$$

where [DNA] is the concentration of DNA in base pairs, the apparent absorption coefficients $\varepsilon_a$, $\varepsilon_f$ and $\varepsilon_b$ correspond to $A_{obs}$/[complex], extinction coefficient for the free complex and the extinction coefficient of the complex in the absolutely bound form respectively. These data were fitted to Eq. (3), with a slope equals to $1/(\varepsilon_b - \varepsilon_f)$ and y-intercept equals to $1/[K_b (\varepsilon_b - \varepsilon_f)]$ and $K_b$ was obtained from the ratio of the slope to the intercept.

*2.3.2. Cyclic voltammetric experiments*

Cyclic voltammetry studies were carried out on a CHI 620C electrochemical analyzer with triple electrode system, glassy carbon as the working electrode, platinum wire as auxiliary electrode and Ag/AgCl as the reference electrode in the medium of 50 mM NaCl, 5 mM Tris buffer (pH 7.2). Solution was deoxygenated by purging with $N_2$ for 30 min prior to measurements.

*2.3.3. Viscosity measurements*

Viscosity experiments were performed with Ostwald viscometer, immersed in a thermostatic water-bath maintained at a constant temperature at 30.0 ± 0.1 °C. CT DNA samples of approximately 0.5 mM were prepared by sonication in order to minimize complexities arising

from CT DNA flexibility [17]. An average flow time was calculated by counting the flow time using a digital stopwatch three times for each sample. Data were used to plot as $(\eta/\eta°)^{1/3}$ *versus* the concentration of the respective metal(II) complex, where η is the viscosity of CT DNA solution in the presence of complex and η° is the viscosity of CT DNA solution in the absence of complex. The relative specific viscosity value was estimated by the equation $\eta = (t-t_0)/t_0$, where $t_0$ is the flow time for the buffer and t is the observed flow time for DNA in the presence and absence of metal complex [18].

*2.4. Antimicrobial screening*

The *in vitro* antimicrobial bustle of $L^1$, $L^2$ and respective complexes was examined against certain human sensitive pathogenic Gram-positive bacteria (*S.aureus* and *B.subtilis*), Gram-negative bacteria (*K.pneumoniae, S.typhi* and *E.coli*) and fungi (*A.niger, F.solani, C.lunata, R.bataticola* and *C.albicans)* using the dilution method [19]. Nutrients like agar and dextrose agar were used as the medium for the growth of bacteria and fungi, whereas kanamycin and fluconazole were chosen as standards for antibacterial and antifungal activity, respectively. These samples were incubated at 37 °C for 24 h (bacteria) and 48 h (fungi), respectively. Each data were collected in terms of MIC (Minimum, Inhibitory Concentration).

*2.5. DNA cleavage efficacy*

Interaction between the ligands and the complexes with pUC18 plasmid DNA was analyzed by agarose gel electrophoresis. Each sample was incubated for 3 h at 37 °C, before the addition of bromophenol blue (0. 25 %), xylene cyanol and glycerol (30 %, 3 μL). The DNA cleavage mixture was subjected to electrophoresis on 1.0 % agarose gel containing 0.3 μM ethidium bromide (EtBr). The gels were run at 50 V for 1 h in TBE (Tris-Borate EDTA) buffer using 1% agarose gel stained with ethidium bromide (1 μg) and the bands were photographed.

**3. Results and discussion**

A series of metal complexes were synthesized and characterized by various physicochemical studies and samples were identified to be stable in air and moisture. These complexes have been characterized by the micro analytical data, FT-IR, UV-Vis, NMR, EPR and mass spectra. These complexes are readily soluble in DMF and DMSO. All the analytical data of

these complexes suggest the proposed general formula $[ML^1_2Cl_2]$/ $[ML^2_2Cl_2]$. Their magnetic susceptibility values of the complexes at room temperature are consistent with octahedral geometry around the central metal ion. The low conductance (10-20 $ohm^{-1}$ $cm^{-2}$ $mol^{-1}$) of the complexes supports their non-electrolytic nature.

### *3.1. FT-IR spectroscopy*

The coordination mode and sites of the ligands to the metal ions were investigated by comparing the infrared spectra of the free ligands ($L^1$ and $L^2$) with their metal complexes. The IR spectra of $L^1$ and $L^2$ and their complexes have been recorded in the region 350-4000 $cm^{-1}$. The spectra of free ligands show a band in the region 1595-1600 $cm^{-1}$, a characteristic feature of the υ(CH=N) (azomethine) stretching mode. This band is shifted towards lower frequency in the spectra of metal complexes 1560-1580 $cm^{-1}$ indicating the involvement of the imine nitrogen in chelation with the metal ion and the lowering of this wave number may be attributed to the decrease in electron density on the nitrogen atom of the azomethine group [20]. Coupled with this, free ligands also reveal a band in the region 1674-1680 $cm^{-1}$ allocated to υ(C=O) stretching mode which is shifted to lower frequency around 1645-1664 $cm^{-1}$ indicating the coordination of the carbonyl oxygen atom of the ligands to metal ion. The coordination of the azomethine nitrogen and carbonyl oxygen is further supported by the appearance of new bands around 505-515 $cm^{-1}$ and 452-464 $cm^{-1}$ which are due to $\upsilon_{(M-O)}$ and $\upsilon_{(M-N)}$ respectively. Furthermore, the IR spectra of all the complexes show an additional band in the region 360 - 374 $cm^{-1}$, which could be perceived due to $\upsilon_{(M-Cl)}$ [21]. The IR spectra of $L^1$ and its Cu(II) complex (**1)** are shown in Fig.S1.

### *3.2. Electronic spectra and magnetic moments*

The free ligands exhibited two intense bands in 35,622–35,714 and 28,952-29,498 $cm^{-1}$ regions due to $\pi \rightarrow \pi^*$ and $n \rightarrow \pi^*$ transitions, respectively [22]. In case of metal complexes, these transitions are shifted to longer wavelengths due to the coordination of the ligand with metal ion. The electronic spectra of Cu(II) complexes (**1** and **5)** displayed d–d transition bands in the region 14,836-14,928 $cm^{-1}$ which can be assigned to $^2E_g \rightarrow {}^2T_{2g}$ transition, characteristic of $d^9$ distorted octahedral geometry [23]. The observed magnetic moment of the Cu(II) complexes (1.84-1.86 BM) at room temperature specify the non-coupled mononuclear complexes of

magnetically diluted $d^9$ system with s = 1/2 spin state of distorted octahedral geometry [24]. In Co(II) complexes (**2** and **6)**, this d-d band emerges at the region 13,247-13,456 $cm^{-1}$ because of $^4T_{1g}(F) \rightarrow {}^4T_{2g}(F)$ transition which can be the evidence for octahedral geometry of $d^7$ Co(II) system. The observed magnetic moment values of these complexes (4.62-4.65 BM) indicate the presence of three unpaired electrons, which suggests an octahedral geometry. The Ni(II) complexes (**3** and **7)** reveal d-d bands in the region 12,654-12,826 $cm^{-1}$, assigned to $^3A_{2g}(F) \rightarrow {}^3T_{1g}(F)$ transition. The examined magnetic moment values of these complexes (3.12-3.35 BM) indicate the presence of two unpaired electrons and octahedral geometry is assigned [25]. In contrast, Zn(II) complexes (**4** and **8)** do not exhibit any d-d band because of their completely filled $d^{10}$ configuration. The electronic absorption spectra of $L^1$ and its Cu(II) complex are depicted in Fig.S2.

### *3.3. $^1H$ and $^{13}C$ NMR spectra*

Both $^1H$ and $^{13}C$ NMR spectra assist to characterize the structure of the prepared ligands and their diamagnetic metal complexes. $^1H$ NMR spectra of free Schiff base ligands and their Zn(II) complexes have been recorded in DMSO-$d_6$. The $^1H$ NMR spectrum of $L^1$ shows peaks at 7.0–7.6 ppm (m) and 6.6 ppm (s), assigned to the phenyl ring protons and (-CH=CH-) of cinnamaldehyde unit respectively. $L^1/L^2$ also shows the following signals: C-$CH_3$ 2.4 ppm (s), N-$CH_3$ 3.2 ppm (s) and azomethine proton (-CH=N) signal at 9.6 ppm (s). The azomethine proton (-CH=N) signal in zinc(II) complexes (**4** and **8)** are found to shift to upfield at 9.4 ppm (s), compared to the free ligands, indicative of the shielding of azomethine group involved in coordination with metal ion. There is no significant change noticed with the remaining signals of complexes, **4** and **8**. The $^1H$ NMR spectra recorded for the Schiff base ligand ($L^1$) and its Zn (II) complex (**4**) are shown in Fig.S3.

The $^{13}C$ NMR spectra of free ligands show aromatic carbon peaks in the range of 125-130 ppm. Moreover, the carbon signals of azomethine (-HC=N) and carbonyl (C=O) groups are observed at 160 and 152 ppm for the free ligands. In case of Zn(II) complexes (**4** and **8)**, it is found that the above peaks are shifted to upfield region, 157 ppm and 144 ppm respectively, supporting the coordination of (-HC=N) and (C=O) groups to the metal center. There is no much difference in other signals of the complexes. The $^{13}C$ NMR spectra of the Schiff base ligand ($L^1$) and its Zn(II) complex (**4)** are given in Fig.S4.

*3.4. EPR spectra*

EPR data of the paramagnetic Cu(II) complex provide evidence on distribution of the unpaired electrons, apparently elucidate the nature of bonding between the metal ion with its ligand. EPR spectra of Cu(II) complexes, dissolved in DMSO were recorded at liquid nitrogen temperature (LNT) and at room temperature (RT). The EPR spectrum of complex **1** is depicted in Fig.S5.

The EPR spectra of Cu(II) complexes (**1** and **5)** exhibit parameters like axially symmetric g-tensor with $g_{II}$ (2.13-2.32) > $g_{\perp}$ (2.03-2.06) > $g_e$ (2.0023); $A_{\parallel}$ (138-152) > $A_{\perp}$(58-85) indicating that the copper site possesses $d_{x^2-y^2}$ ground state, characteristic of an octahedral geometry [26]. The geometric parameter G refers to a measure of the exchange interaction among the multiple copper centers in the polycrystalline compound. It is calculated by the following equation:

$$G = (g_{II} - 2) / (g_{\perp} - 2) \quad \text{.....(3)}$$

As per earlier report, if value of G > 4.0, the local tetragonal axes exist in parallel alignment or slightly misaligned. In case value of G < 4.0, significant exchange coupling occurs and there is significant deviation. While the observed values for the exchange interaction parameter of Cu(II) complexes fall within the range of 4.3-5.3 G which suggests that the local tetragonal axes are aligned in parallel or slightly deviated and the unpaired electron occupies in the $d_{x^2-y^2}$ orbital. At this state, it infers the absence of exchange coupling among the Cu(II) centers in solid state [27].

The empirical ratio of $g_{\parallel}/A_{\parallel}$ is often used to detect the distortion in Cu(II) complexes. If this ratio is close to 100, it indicates approximately a square-planar assembly around the Cu(II) ion and if the values around 170 – 250 which support the distorted tetrahedral geometry. In case if the ratio is existing within 110-170, it specifies almost an octahedral coordination around Cu(II) ion with minor distortion [28]. For the synthesized Cu(II) complexes, the values of $g_{\parallel}/A_{\parallel}$ are found to be 152 $cm^{-1}$ (**1**) and 154 $cm^{-1}$ (**5**) which infer that Cu(II) complexes reveal the distorted octahedral geometry. The calculated spin Hamiltonian parameters for the Cu(II) complexes are listed in Table 1.

(Kindly insert Table 1 here)

*3.5. Mass spectra*

The electrospray ionization - mass spectra (ESI-MS) were recorded at room temperature for the synthesized Schiff base ligands and the corresponding metal complexes. The molecular ion peak and fragmentation observed in ESI-MS support the proposed formulae for the synthesized metal complexes. ESI-MS of the free ligand ($L^1$) and complex **1** are depicted in Fig.S6. The mass spectrum of $L^1$ shows the molecular ion peak at m/z 317 corresponding to $[C_{20}H_{19}N_3O]^+$, in addition to the fragmentation peaks at m/z 214, 187, 103, 77 and 65 which are attributed to the species, $[C_{12}H_{12}N_3O]^+$, $[C_{11}H_{11}N_2O]^+$, $[C_8H_7]^+$, $[C_6H_5]^+$ and $[C_5H_5]^+$ respectively. The mass spectrum of complex **1** shows molecular ion peaks at m/z 770 $[M^{+1}]$, which corresponds to its molecular weight. The fragmentation of $[CuC_{40}H_{38}N_6O_2Cl_2]^{+1}$ leads to the elimination of two chloride ions followed by the demetallation based on evidence of m/z values, 699 and 606 with respect to the fragmented ions $[CuC_{40}H_{38}N_6O_2]^+$ and $[C_{40}H_{38}N_6O_2]^+$ respectively. The intense peak (base peak) at m/z 317 represents the stable species $[C_{20}H_{19}N_3O]^+$ from the ligand moiety. Moreover, the fragmentation peaks in the spectrum at m/z 214, 187 and 103 support the existence of $[C_{12}H_{12}N_3O]^+$, $[C_{11}H_{11}N_2O]^+$ and $[C_8H_7]^+$ respectively. Also, m/z values of all the fragments of $L^1$ and its copper(II) complex determine the stoichiometry of the complexes which is found to be $[ML^1{}_2Cl_2]$. Thus, all the observed peaks reveal a good agreement with the formula estimated from micro analytical data. Altogether, ESI-MS data support the conclusion drawn from the analytical and conductance values.

*3.6. DNA binding studies*

*3.6.1 Absorption spectral titration*

Absorption titration is universally employed to monitor the binding mode and propensity of drugs with nucleic acid [29]. The change in the absorbance and shift in the wavelength at UV-visible region due to the addition of calf thymus DNA (CT DNA) to metal complex solution indicates the nature of interaction of the complexes with DNA. Thus the absorption spectra of these complexes in the absence or presence of CT DNA at different concentrations were measured. ‘‘Hyperchromic effect’’ and ‘‘hypochromic effect’’ are two types of spectral features of DNA, concerning its double-helix structure. This effect of spectral feature reveals the respective alternation of DNA in its conformation and structure while the drug binds to DNA. Hypochromism results from the contraction of DNA in the helix axis as well as from the change

in conformation on DNA, while hyperchromism results from the damage of the DNA double helix structure [30]. With the increase of [DNA], the absorption intensity of the complex decreases (hypochromic effect) and the $\lambda_{max}$ values shift to red region (bathochromic shift) [31]. This occurs while the binding induces a strong stacking interaction between the planar aromatic chromophoric groups of the ligand with DNA base pairs.

The absorption spectra of all the complexes showed an intensive absorption band in the region 336-348 nm, in 5 mM Tris-HCl/50 mM NaCl (pH 7.2) buffer solution. The observed hypochromicity values in the presence of DNA were in the range 10.2–15.8 % for MLCT band and their red shifts were observed in the region 3.0-8.0 nm which indicates the binding of DNA with the complexes is through intercalative mode [32]. The absorption spectra of the complexes **1** and **3** in the absence and presence of CT DNA in the UV region are depicted in Fig.1.

(Kindly insert Fig.1 here)

The intrinsic binding constant $K_b$ values calculated from the slope to the intercept ratio from the plots between [DNA]/ ($\varepsilon_b$- $\varepsilon_f$) and [DNA] are given in Table 2 and used to gather the information concerning the binding affinity of the complexes with CT DNA. The binding strength of the complexes is shown as in the following order: **1**>**3**>**4**>**2**>5>**6**>**8**>**7**>**.** Complex **1** reveals strong hypochromism and a slight red shift as compared to other complexes highlighting its higher DNA binding propensity. These results imply that the intercalative ligands with extended aromatic plane and good conjugation effect can greatly support the DNA binding facility. The determined intrinsic binding constants for all the complexes are recline within the range 1.2-8.6 × $10^4$ $M^{-1}$. Comparing the values of $K_b$ of the metal complexes with the classical intercalators, these complexes have lesser binding affinity than the classical intercalators such as EB [33] and higher than those of some Schiff base metal complexes [34] indicating that the present complexes strongly bind with DNA through an intercalation mode into the double helix structure of DNA.

(Kindly insert Table 2 here)

*3.6.2 Viscosity measurements*

Hydrodynamic method, such as determination of viscosity, which is exquisitely sensitive to the change of length of DNA, may be the most effective means studying the binding mode of complexes to DNA in the absence of X-ray crystallographic data [35]. The relative specific viscosity of DNA is determined by varying the concentration of the added metal complexes.

Measuring the viscosity of DNA is a classical technique used to analyze the DNA binding mode in solution. Under appropriate conditions, intercalation of drugs such as ethidium bromide [EB] causes a significant increase in the viscosity of a DNA solution due to the increase in the separation of the base pairs of the intercalation sites and hence, results in an increase in the overall DNA contour length [36], as shown in Fig.2. In contrast, partial or non-classical intercalation of complex would bend or kink the DNA helix, shortening the effective length of the DNA and reducing DNA viscosity accordingly, while the electrostatic and groove binding cause little or no effect on the relative viscosity of DNA solution [37].

(Kindly insert Fig.2 here)

Viscosity measurements results clearly show that all the complexes can intercalate between adjacent DNA base pairs, causing an extension in the helix thereby increasing the viscosity of DNA. Increasing tendency in the viscosity curve upon addition of various concentrations of complex to DNA provided stronger evidence for the intercalation and further verified intercalative mode of binding as investigated through spectroscopic and electrochemical studies in the present work.

*3.6.3 Electrochemical studies*

Electrochemical investigation of drug–DNA interactions can provide a useful complement to other methods and yield information about the mechanism of interaction and the conformation of adduct [38]. In general, the electrochemical potential of a small molecule will shift positively while it intercalates with DNA double helix, and it will shift to negative direction, if the molecule is bound to DNA by groove binding [39]. In the present study, cyclic voltammetry technique has been used to find out the nature of DNA binding mode of the metal complex. The cyclic voltammograms of the complexes **1** and **4** in the absence and presence of varying amount of DNA are shown in Fig.3.

(Kindly insert Fig. 3 here)

The cyclic voltammogram of each complex shows approximately close to unity for peak current ratio, which is responsible for the reaction of the complex on the glassy carbon as the quasi-reversible redox process. The incremental addition of CT DNA to the complex causes decrease in anodic and cathodic peak current of the complex. This result shows that complex stabilizes the duplex (GC pairs) as an intercalating manner. The drop of the voltammetric current in the presence of CT DNA is due to slow diffusion of the copper complex bound to CT DNA.

The formal potential, $E_{1/2}$, taken as the average of Ep*c* and Ep*a* shifts slightly towards the positive side on binding to DNA which suggests that copper complex binds intercalative to CT DNA [40]. The quasi- reversible redox couple for each complex in DMSO solution has been analyzed upon addition of CT DNA. The $E_{1/2}$ and ΔEp values are given in Table 3.

(Kindly insert Table 3 here)

*3.7. Antimicrobial screening*

The *in vitro* antimicrobial activity of the synthesized free ligands and their metal complexes were tested against perceptive organisms such as two Gram-positive bacteria (*Staphylococcus aureus* and *Bacillus subtilis)* and three Gram-negative bacteria (*Escherichia coli, Klebsiella pneumoniae* and *Salmonella typhi*) and five fungi (*Aspergillus niger, Fusarium solani*, *Curvularia lunata, Rhizoctonia bataticola* and *Candida albicans*) by well dilution method. Kanamycin and fluconazole were used as standards for bacteria and fungi respectively. The minimum inhibitory concentration (MIC) values, measured in antibacterial and antifungal studies of the complexes are given in Tables 4 and 5.

(Kindly insert Tables 4 and 5 here)

It is observed that the activity of imine ligand is enhanced when coordinated to the metal ions. The presence of imine group (-C=N) and chelation effect with central metal enhance the antimicrobial action [41]. Moreover, it has been already proved that the ligand containing nitrogen and oxygen donor systems might restrain enzyme production, since the enzymes which require these groups for their activity appear to be especially more susceptible to deactivation by the metal ion upon chelation. The presence of nitrogen and oxygen atoms may also be the higher biocidal actions of the metal complexes. This enhancement of antimicrobial activity of these metal complexes may be explained by Overtone concept and Tweedy′s chelation theory [42]. According to the Overtones concept, chelation reduces the polarity of the metal ion mainly because of partial sharing of its positive charge with donor groups within the whole chelating system. This process of chelation thus increases the lipophilic nature of the central metal atom, which in turn, favors its permeation through the lipoid layer of the membrane thus causing the metal complex to cross the bacterial membrane more effectively, which in turn increases the activity of the complexes. These complexes also disturb the respiration process of the cell and thus block the synthesis of proteins, which restricts further growth of organisms [43]. The

complex **1** showed highest antimicrobial activity among all the other complexes. The variation in the effectiveness of different compounds against different organisms depends either on the impermeability of the cells of the microbes or on differences in ribosome of microbial cells [44]. Besides this, many other factors such as solubility, dipole moment and conductivity of complexes may be the reason for remarkable antimicrobial activities of the complexes.

*3.8. DNA cleavage study*

DNA cleavage is controlled by the relaxation of supercoiled circular form of pUC18 DNA into nicked circular and linear forms. When circular plasmid DNA in the presence of metal complex is subjected to electrophoresis, relatively fast migration will be viewed for the intact supercoiled form (Form I). If scission occurs on one strand, the super coil will relax to turn out a slower moving open circular form (Form II). If both the strands are cleaved, a linear form (Form III) that migrates in between Form I and II will be generated [45].

The DNA cleavage ability of the complexes (**1-4**) has been investigated by gel electrophoresis using supercoiled pUC18 DNA in TBE buffer in the presence of $H_2O_2$ at 35°C for 5h. As seen from Fig.4, the control experiments with DNA alone (lane 1) and DNA in presence of $L^1$ (lane 2) do not show any cleavage activity. Obviously the complexes (**1-4**) are found to exhibit nuclease activity. Thus the cleavage of super coiled form-I to the open circular form-II is induced by all the metal complexes, in which the complexes **1, 3** and **4** exhibit prominent cleavage activity than complex **2**. The cleavage mechanism is explained as follows. When the redox-active metal complexes interact with biomolecules in the presence of $H_2O_2$ as an oxidizing agent, it is believed to produce different oxygen intermediates (reactive oxygen species) depending on different metal complexes and conditions. The metal complexes in the presence of $H_2O_2$ may produce reactive hydroxyl radical ($OH^*$) that can cleave the deoxyribose moiety, followed by hydrolytic cleavage of a sugar phosphate back bone [46]. It may also be concluded that complexes which cleave the DNA may also inhibit the growth of the pathogenic organism.

(Kindly insert Fig.4 here)

## Conclusion

Synthesis and characterization of a new set of pyrazolone precursor Schiff bases and a series of transition metal(II) complexes of Cu, Zn, Co and Ni are reported as potential candidates to study their DNA binding/cleavage and antimicrobial effects. The physicochemical and spectral data infer that all these metal chelates (**1-8**) exist as mononuclear and adopted octahedral geometry around the metal center. DNA binding properties of all the above complexes were studied by electronic absorption spectra, cyclic voltammetry and viscosity measurement, which deduce their association as intercalative DNA interaction with different binding affinities. The binding strength of these complexes with DNA varies by the following order, **1**>**3**>**4**>**2**>**5**>**6**>**8**>**7**. Gel electrophoresis experiments infer that DNA cleavage is enhanced to significant extent in the presence of hydrogen peroxide. Active oxygen intermediate like hydroxyl radicals generated from hydrogen peroxide upon cleavage mechanism could play an important role. Compared to antibacterial and antifungal activities of the free ligands, their complexes show efficient biocidal and fungicidal activity. Based on the summary of results, promising candidates are identified for further investigation towards the direction of exploring new and potential drug for cancer therapeutics.

## Acknowledgments

The authors express their heartfelt thanks to the College Managing Board, Principal and Head of the Department of Chemistry, VHNSN College (Autonomous), Virudhunagar for providing necessary research facilities. IIT Bombay (SAIF) and IIT Chennai, India are gratefully acknowledged for providing instrumental facilities.

**References**


1. A.A. Al-Amiery, A.A.H. Kadhum, A.B. Mohamad, Bioinorg. Chem. Appl. 2012 (2012) 1-6.
2. B. Anupama, C. Gyana Kumari, Res. J. Pharm. Biol. Chem. Sci. 2 (2011) 140-159.
3. J.Tisato, F.Refosco, F.Bandoli, Coord. Chem. Rev.135 (1994) 325-397.
4. N. Raman, A. Kulandaisamy, A. Shanmugasundaram, Transit. Metal. Chem. 26 (2001) 131-135.
5. M.M. El-ajaily, R.M. El-Ferjani, A.A. Maihub, Jordan J. Chem. 2 (2007) 287-296.
6. T. Rosu, E. Pahontu, C. Maxim, R. Georgescu, N. Stanica, G.L. Almajan, A. Gulea, Polyhedron 29 (2010) 757-766.
7. N. Arshad, M. Ahmad, M.Z. Ashraf, H. Nadeem, J. Photochem. Photobiol. B 138 (2014) 331-346.
8. J.S. Casas, M.S. García-Tasende, A. Sánchez, J. Sordo, A. Touceda, Coord. Chem. Rev. 251 (2007) 1561-1589.
9. N.V. Bashkatova, E.I. Korotkova, Y.A. Karbainov, A.Y. Yagovkin, A.A. Bakibaev, J. Pharm. Biomed. Anal. 37 (2005) 1143-1147.
10. S.S. Abd El Rehim, M.A.M. Ibrahim, K.F. Khalid, Mater. Chem. Phys. 70 (2001) 268-273.
11. M.S. Collado, V.E. Mantovani, H.C. Goicoechea, A.C. Olivieri, Talanta. 52 (2000) 909-920.
12. J. Parekh, P. Inamdhar, R. Nair, S. Baluja, S. Chanda, J. Serb. Chem. Soc. 70 (2005) 1155-1158.
13. R. Paul Pandiyan, T. Arun, N. Raman, S. K. Shanuja, A. Gnanamani, Int. J. Inorg. Bioinorg. Chem. 6 (2016) 23-34.
14. P. Krishnamoorthy, P. Sathyadevi, P.T. Muthiah, N. Dharmaraj, RSC Adv. 2 (2012) 12190-12203.
15. M.E. Reichmann, S.A. Rice, C.A. Thomas, P. Doty, J. Am. Chem. Soc. 76 (1954) 3047–3053.
16. K.E. Heim, A.R. Tagliaferro , D.J. Bobilya, *J. Nutr. Biochem*., 13 (2002) 572-584.
17. S. Satyanarayana, J.C. Dabrowiak, J.B. Chaires, Biochemistry 32 (1993) 2573–2584.
18. G. Cohen and H. Eisenberg, Biopolymers 8 (1969) 45-55.

19. M. Ganeshpandian, S. Ramakrishnan, M. Palaniandavar, E. Suresh, A. Riyasdeen, M.A. Akbarsha, J.Inorg. Biochem. 140 (2014) 202-212.
20. Z.H.A. El-Wahab, M.M. Mashaly, A.A. Salman, B.A. El-Shetary, A.A. Faheim, Spectrochim. Acta A 60 (2004) 2861-2873.
21. P.P. Dholakiya, M.N. Patel, Inorg. Met.-Org. Nano-Met. Chem. 32 (2002) 819–829.
22. R. Holman, M.P. Hendrich, L.Q. Jr, *Inorg. Chem.* 31 (1992) 937-939.
23. Y. Prashanthi, K. Kiranmai, N.J.P. Subhashini, P. Shivaraj, Spectrochim. Acta A 70 (2008) 30-35.
24. A.B.P. Lever, Inorganic Electronic Spectroscopy, Elsevier, Amsterdam, 2nd edition, 1984.
25. S.S. Konstantinovic, B.C. Radovanovic, A. Krkljes, J. Therm. Anal. Calorim. 90 (2007) 525-531.
26. G. Speier, J. Csihony, A.M. Whalen, C.G. Pierpont, Inorg. Chem. 35 (1996) 3519-3524.
27. R.J. Dudleyand, B. Hathaway, J. Chem. Soc. A 12 (1970) 2794-2799.
28. B.J. Hathaway, D.E. Billing, Coord. Chem. Rev. 5 (1970) 143-207.
29. J. Ravichandran, P. Gurumoorthy, M.A. Imran Musthafa, A. Kalilur Rahiman, Spectrochim. Acta A 133 (2014) 785–793.
30. Q.S. Li, P. Yang, H.F. Wang, and M. L. Guo, J. Inorg. Biochem. 64 (1996) 181–195.
31. H. Chao, W.J. Mei, Q.W. Huang, L.N. Ji, J. Inorg. Biochem. 92 (2002) 165-170.
32. S. Zhang, J. Zhou, J. Coord. Chem. 61 (2008) 2488-2498.
33. M.J. Waring, J. Mol. Biol. 13 (1965) 269-282.
34. T. Kiran, V.G. Prasanth, M.M. Balamurali, C.S. Vasavi, P. Munusamy, M. Pathak, Inorg. Chim. Acta 433 (2015) 26-34.
35. F.H. Li, G.H. Zhao, H.X. Wu, H. Lin, X.X. Wu, S.R. Zhu, H.K. Lin, J. Inorg. Biochem. 100 (2006) 36-43.
36. A. Srishailam, N.M.Gabra, Y.P. Kumar, K.L. Reddy, C.S. Devi, D. Anil Kumar, S.S. Singh, S. Satyanarayana, J. Photochem. Photobiol. B 141 (2014) 47–58.
37. B.D. Wang, Z.Y. Yang, P. Crewdson, D.Q. Wang, *J. Inorg. Biochem.* 101 (2007) 1492–1504.
38. M.S. Ibrahim, Anal. Chim. Acta, 443 (2001) 63-72.

39. K. Nagaraj, G. Velmurugan, S. Sakthinathan, P. Venuvanalingam, Dalton Trans. 43 (2014) 18074-18086.
40. J. Annaraj, S. Srinivasan, K.M. Ponvel, P.R. Athappan, J. Inorg. Biochem. 99 (2005) 669–676.
41. P. Mendu_, C.G. Kumari, R. Ragi, J. Fluoresc. 25 (2015) 369-378.
42. B.G. Tweedy, Phytopathology, 55 (1964) 910-914.
43. R.R. Coombs, S.A. Westcott, A. Decken, F.J. Baerlocher, Transit. Met. Chem. 30 (2005) 411–418.
44. A.E. El-Tabl, F.A. EL-Saied, W. Plass, A.N. Al-Hakimi, Spectrochim. Acta A 71 (2008) 90–99.
45. D.D. Li, J.L. Tian, W. Gu, X. Liu, S.P. Yan, Eur. J. Inorg. Chem. 2009 (2009) 5036-5045.
46. M. Ganeshpandian, R. Loganathan, E. Suresh, A. Riyasdeen, M.A. Akbarshad, M. Palaniandavar, Dalton Trans. 43 (2014) 1203-1219.

**Figure captions**

**Scheme 1.** The formation of Schiff base ligands $L^1$ and $L^2$

**Scheme 2.** Schematic route for the synthesis of metal complexes using Schiff base ligands ($L^1$/$L^2$)

**Fig.1** The absorption spectra of the complexes (**1**) and (**3**) in buffer pH =7.2 at $25^0$ C in presence of increasing amount of DNA. Arrow indicates the changes in absorbance upon increasing the DNA concentration.

**Fig.2** Effect of increasing amount of [EB] (∗), Complexes **1** (♦), **2** (■), **3**(▲) and **4** (×) on the relative viscosity of CT DNA. Plot of relative viscosity $(\eta/\eta o)^{1/3}$ *vs* [Complex]/[DNA].

**Fig.3** The cyclic voltammograms of the complexes **1** and **4** in buffer (pH = 7.2) at $25^0$C in presence of increasing amount of DNA.

**Fig.4** Gel electrophoresis pattern showing cleavage of pUC18 DNA treated with metal complexes. Lane I: DNA control; Lane II: DNA + $L^1$+ $H_2O_2$; Lane III: DNA + **1** + $H_2O_2$; Lane IV: DNA + **2** + $H_2O_2$; Lane V: DNA + **3** + $H_2O_2$ and Lane VI: DNA + **4** + $H_2O_2$.

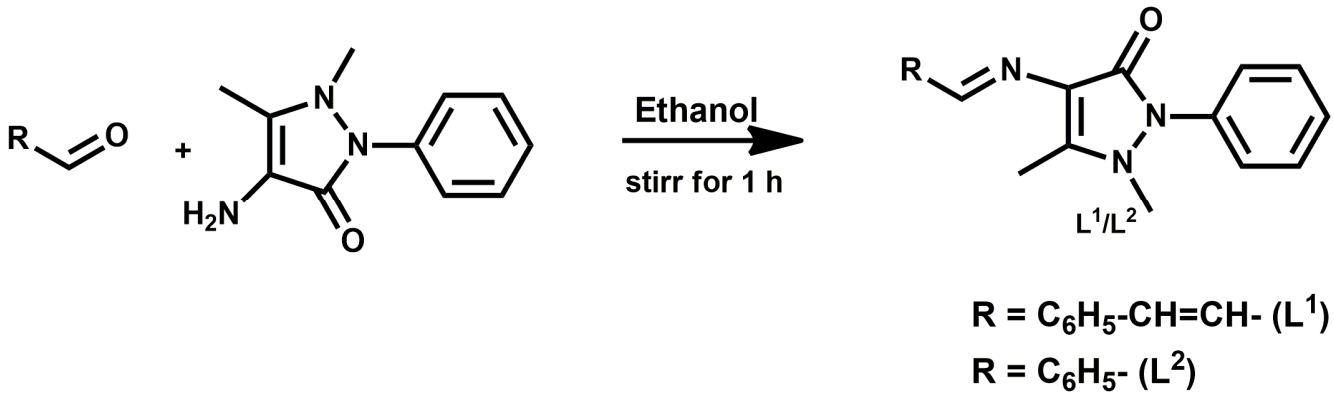


**Scheme 1.** The formation of Schiff base ligands $L^1$ and $L^2$

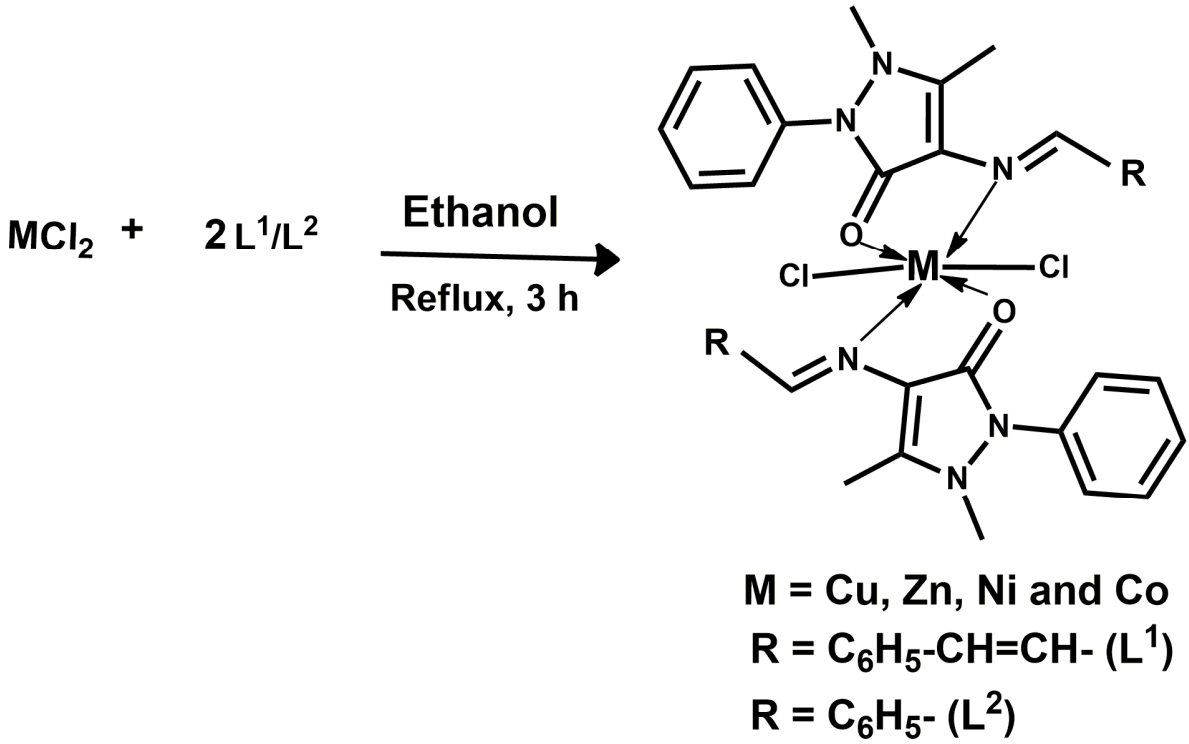


**Scheme 2.** Schematic route for the synthesis of metal complexes using Schiff base ligands ($L^1/L^2$)

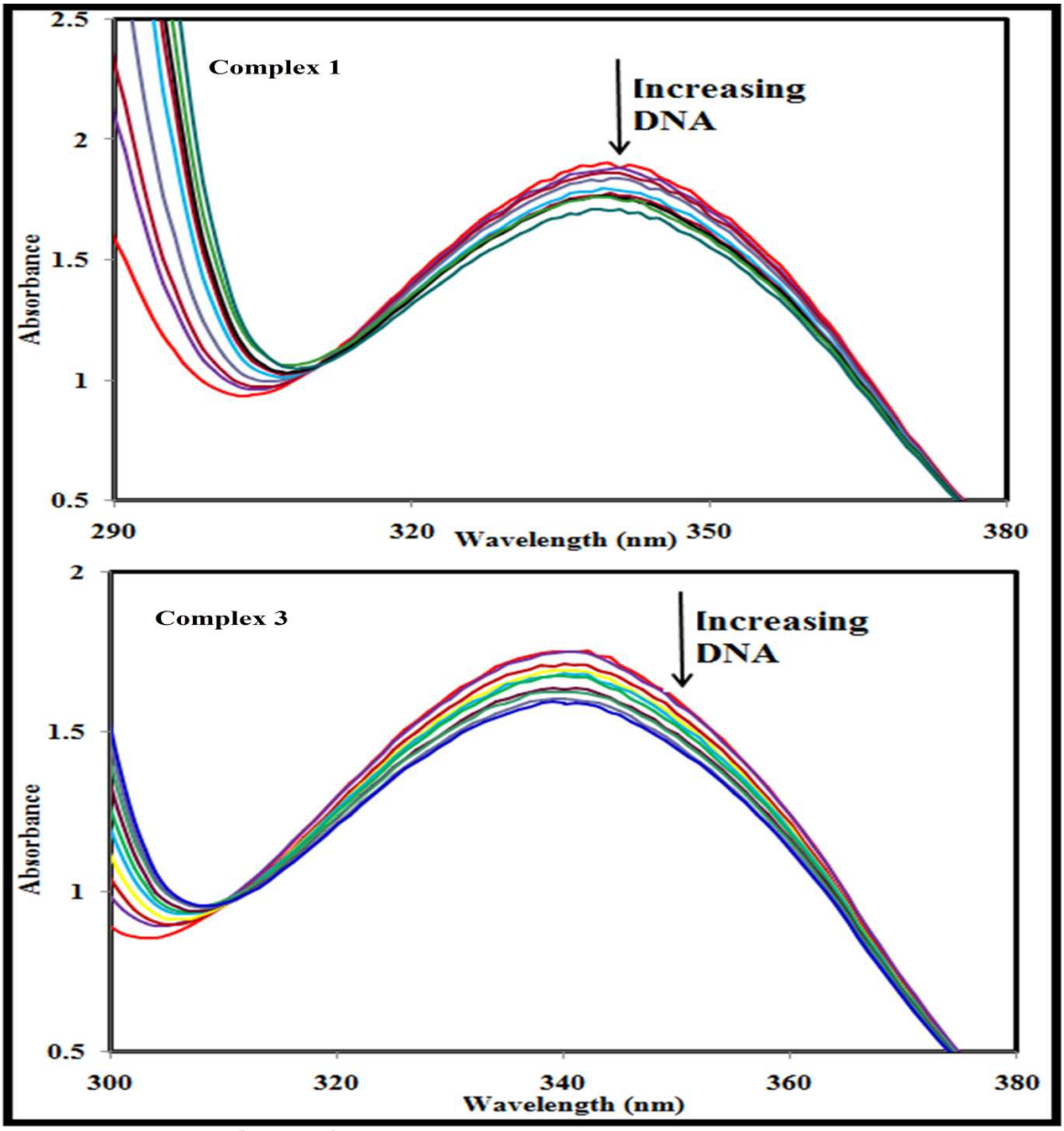


**Fig.1** The absorption spectra of the complexes (**1**) and (**3**) in buffer pH =7.2 at 25$^0$C in presence of increasing amount of DNA. Arrow indicates the changes in absorbance upon increasing the DNA concentration.

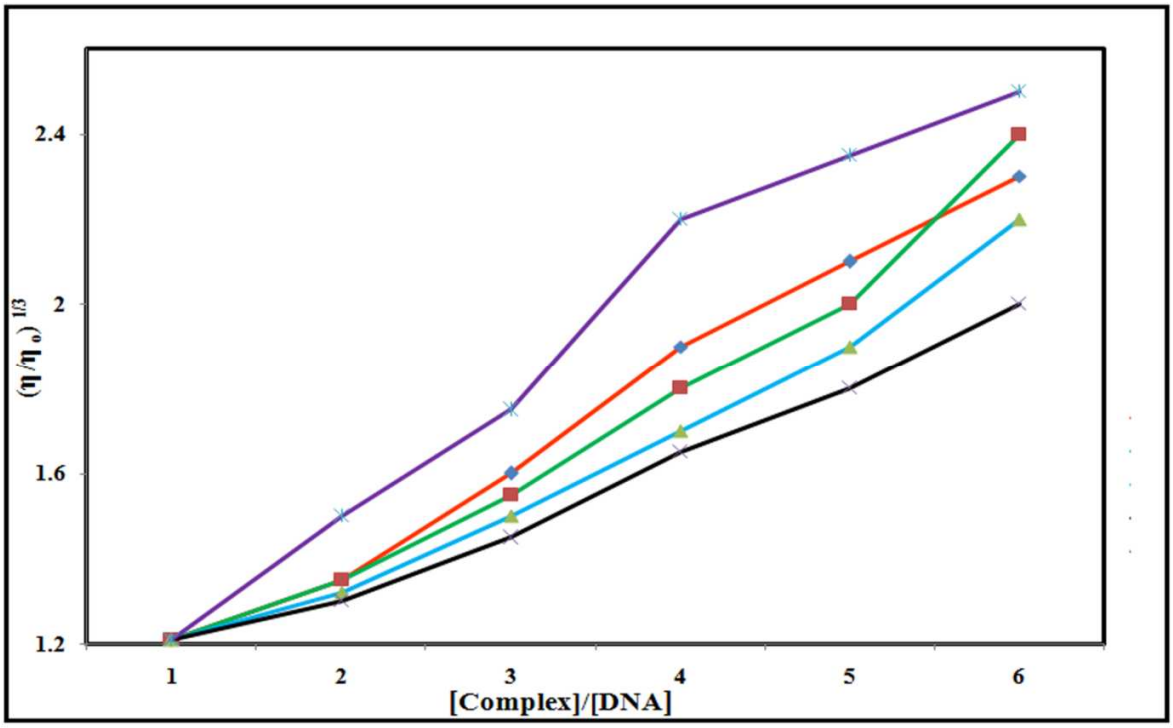


**Fig.2** Effect of increasing amount of [EB] (∗), Complexes **1** (♦), **2** (■), **3**(▲) and **4** (×) on the relative viscosity of CT DNA. Plot of relative viscosity $(\eta/\eta o)^{1/3}$ *vs* [Complex]/[DNA].

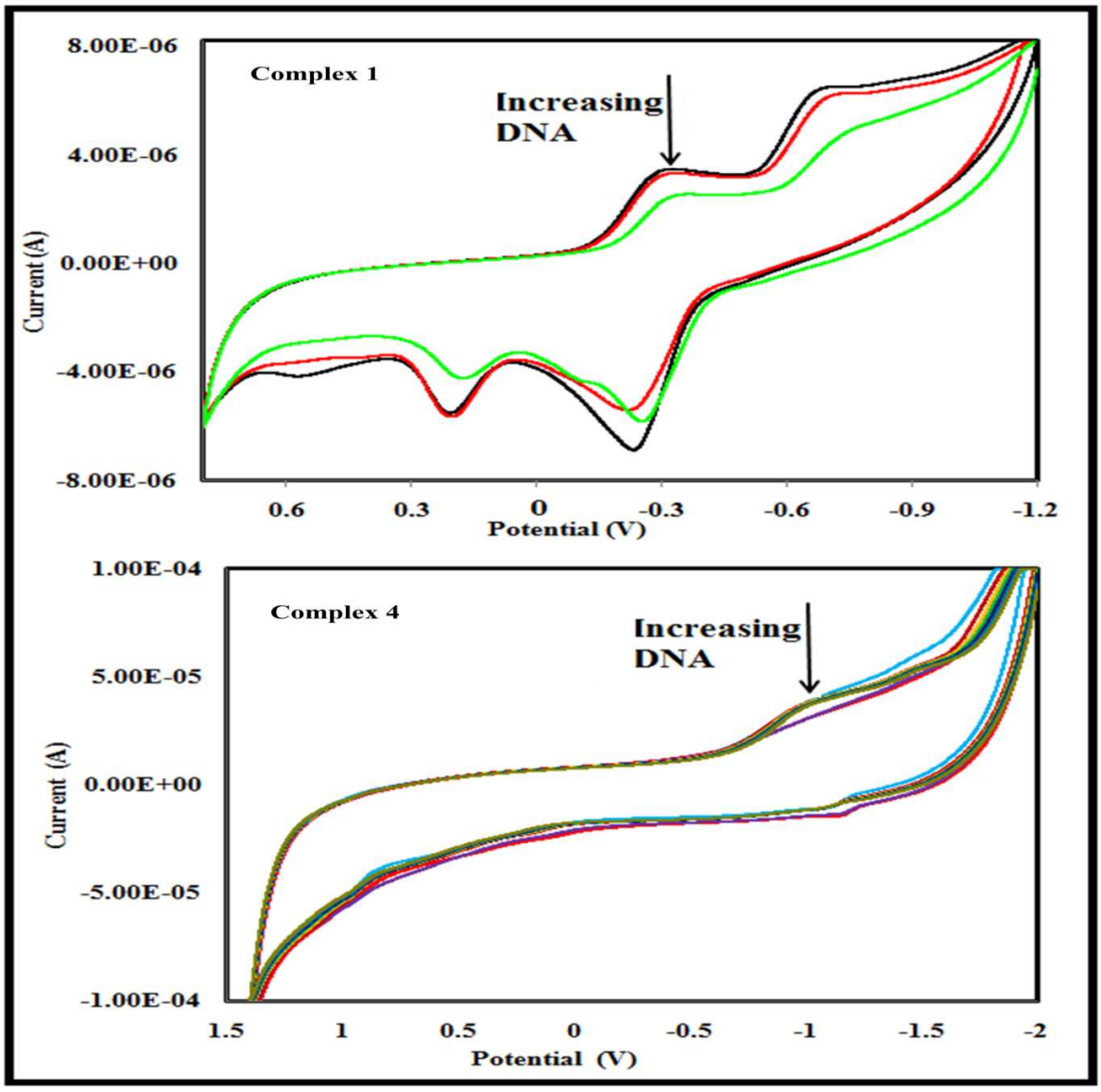


**Fig.3** The cyclic voltammograms of the complexes **1** and **4** in buffer (pH = 7.2) at $25^0$C in presence of increasing amount of DNA.

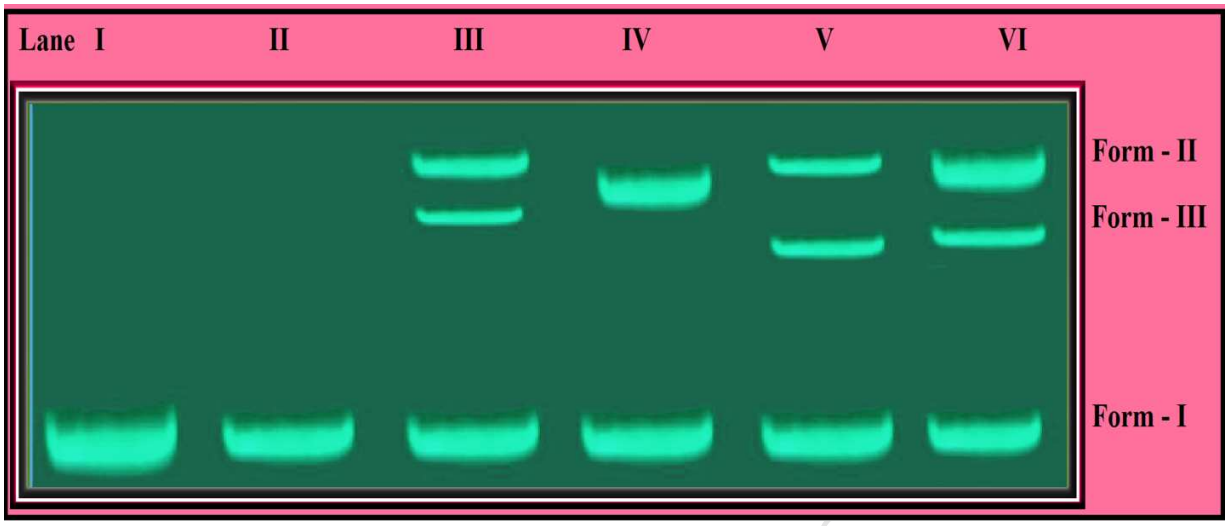


**Fig.4** Gel electrophoresis pattern showing cleavage of pUC18 DNA treated with metal complexes. Lane I: DNA control; Lane II: DNA + $L^1$+ $H_2O_2$; Lane III: DNA + **1** + $H_2O_2$; Lane IV: DNA + **2** + $H_2O_2$; Lane V: DNA + **3** + $H_2O_2$ and Lane VI: DNA + **4** + $H_2O_2$.

**Table Captions**

**Table 1.** The spin Hamiltonian parameters of the Cu(II) complexes (1 and 5) in DMSO solution at LNT.

**Table 2.** Electronic absorption parameters for the interaction of DNA with synthesized metal complexes.

**Table 3.** Electrochemical parameters for the interaction of DNA with synthesized metal complexes.

**Table 4.** Minimum inhibitory concentration of the synthesized free ligands and metal complexes against the growth of bacteria (μM).

**Table 5.** Minimum inhibitory concentration of the synthesized free ligands and metal complexes against the growth of fungi (μM).

**Table 1.** The spin Hamiltonian parameters of the Cu(II) complexes (1 and 5) in DMSO solution at LNT.

| Complex | g-tensor | | | $A \times 10^{-4}$ ($cm^{-1}$) | | | $g_{\|/} A_{\|}$ | G |
|---|---|---|---|---|---|---|---|---|
| | $g_{\|}$ | $g_{\perp}$ | $g_{iso}$ | $A_{\|}$ | $A_{\perp}$ | $A_{iso}$ | | |
| **1** | 2.32 | 2.06 | 2.15 | 152 | 85 | 107 | 152 | 5.3 |
| **5** | 2.13 | 2.03 | 2.06 | 138 | 58 | 85 | 154 | 4.3 |

**Table 2.** Electronic absorption parameters for the interaction of DNA with synthesized complexes.

| Complex | λ max | | Δλ (nm) | [a]H% | $K_b \times 10^4$ ($M^{-1}$) |
|---|---|---|---|---|---|
| | Free | Bound | | | |
| 1 | 336 | 342 | 6 | 15.8 | 8.6 |
| 2 | 338 | 342 | 4 | 10.8 | 4.5 |
| 3 | 336 | 341 | 5 | 13.5 | 6.4 |
| 4 | 348 | 352 | 4 | 10.2 | 5.2 |
| 5 | 332 | 340 | 8 | 14.3 | 4.4 |
| 6 | 342 | 348 | 6 | 12.8 | 3.2 |
| 7 | 338 | 341 | 3 | 13.8 | 1.2 |
| 8 | 342 | 350 | 8 | 14.2 | 2.2 |

[a]H% = $[(A_{free} - A_{bound}) / A_{free}] \times 100\%$

**Table 3.** Electrochemical parameters for the interaction of DNA with synthesized metal complexes.

| Complex | $E_{1/2}(V)^a$ | | $^b\Delta Ep(V)$ | | $Ip_a/Ip_c$ |
|---|---|---|---|---|---|
| | Free | Bound | Free | Bound | |
| **1** | -0.305 | -0.265 | 1.458 | 2.148 | 0.82 |
| **2** | -0.305 | -0.265 | 1.458 | 2.148 | 0.82 |
| **3** | -0.552 | 0.238 | 1.146 | 2.268 | 0.88 |
| **4** | 0.404 | 0.638 | 3.301 | 3.402 | 0.96 |
| **5** | -0.189 | -0.061 | 1.759 | 1.782 | 0.89 |
| **6** | 0.826 | 0.832 | 0.585 | 0.482 | 0.96 |
| **7** | -0.090 | 0.351 | 1.466 | 2.011 | 0.82 |
| **8** | 0.778 | 0.912 | 1.557 | 1.627 | 0.69 |

Data from cyclic voltammetric measurements: $^aE_{1/2}$ is calculated as the average of anodic ($E_{Pa}$) and cathodic ($E_{pc}$) peak potentials; $E_{1/2}{}^a = E_{Pa} + E_{pc} / 2$ ; $^b\Delta Ep = E_{pa} - E_{pc}$

**Table 4.** Minimum inhibitory concentration of the synthesized free ligands and metal complexes against the growth of bacteria (μM).

| Compound | Minimum inhibitory concentration ( × $10^4$ μM) | | | | |
|---|---|---|---|---|---|
| | ***Staphylococcus aureus*** | ***Bacillus subtilis*** | ***Escherichia coli*** | ***Klebsiella pneumoniae*** | ***Salmonella typhi*** |
| **$L^1$** | 25.8 | 22.4 | 28.6 | 26.8 | 30.5 |
| **$L^2$** | 26.5 | 25.2 | 30.8 | 28.2 | 32.4 |
| **1** | 10.4 | 10.8 | 11.5 | 10.2 | 12.2 |
| **2** | 12.6 | 14.5 | 13.4 | 14.2 | 12.8 |
| **3** | 11.8 | 10.8 | 12.8 | 14.8 | 12.2 |
| **4** | 10.8 | 12.2 | 11.2 | 11.5 | 12.8 |
| **5** | 11.5 | 11.8 | 12.2 | 10.8 | 12.8 |
| **6** | 12.8 | 11.5 | 13.6 | 15.8 | 13.6 |
| **7** | 11.2 | 12.8 | 12.2 | 11.8 | 13.8 |
| **8** | 12.0 | 12.8 | 12.6 | 11.8 | 13.5 |
| [a]Kanamycin | 2.4 | 2.2 | 1.8 | 2.8 | 3.2 |

[a]Kanamycin is used as standard

**Table 5.** Minimum inhibitory concentration of the synthesized free ligands and metal complexes against the growth of fungi (μM).

| Compound | Minimum inhibitory concentration ( × $10^4$ μM) | | | | |
|---|---|---|---|---|---|
| | ***Aspergillus niger*** | ***Fusarium solani*** | ***Curvularia lunata*** | ***Rhizoctonia bataticola*** | ***Candida albicans*** |
| **$L^1$** | 18.8 | 16.2 | 15.8 | 17.5 | 16.0 |
| **$L^2$** | 20.5 | 18.6 | 17.5 | 18.4 | 18.8 |
| **1** | 6.8 | 7.6 | 7.2 | 8.4 | 8.2 |
| **2** | 9.2 | 8.7 | 8.6 | 9.0 | 7.8 |
| **3** | 8.6 | 9.4 | 8.4 | 8.8 | 8.2 |
| **4** | 7.4 | 8.3 | 8.8 | 8.4 | 7.2 |
| **5** | 8.5 | 9.6 | 7.8 | 9.2 | 9.6 |
| **6** | 10.5 | 10.2 | 9.8 | 10.8 | 9.5 |
| **7** | 9.5 | 10.2 | 10.6 | 9.5 | 9.8 |
| **8** | 10.0 | 11.2 | 9.5 | 9.2 | 10.5 |
| [a]Fluconazole | 4.2 | 4.5 | 3.2 | 3.8 | 4.8 |

[a]Fluconazole is used as standard

## Research Highlights

- Synthesis and characterization of biosensitive pyrazolone precursor complexes.
- Mononuclear and octahedral geometry around the central metal ion.
- Evidence for metallointercalation by *in vitro* DNA binding studies.
- Higher DNA nuclease efficacy of the complexes than the free ligands.
- Excellent *in vitro* antimicrobial performance against various pathogens.